International Journal of Nanomedicine

Dovepress
open access to scientific and medical research

Open Access Full Text Article

ORIGINAL RESEARCH

Mn^{2+}-coordinated PDA@DOX/PLGA nanoparticles as a smart theranostic agent for synergistic chemo-photothermal tumor therapy

This article was published in the following Dove Press journal:
International Journal of Nanomedicine
24 April 2017
Number of times this article has been viewed

Juqun Xi[1–3]
Lanyue Da[1]
Changshui Yang[1]
Rui Chen[4]
Lizeng Gao[2]
Lei Fan[5]
Jie Han[5]

[1]Pharmacology Department, Medical School, Yangzhou University, [2]Jiangsu Key Laboratory of Integrated Traditional Chinese and Western Medicine for Prevention and Treatment of Senile Diseases, [3]Jiangsu Co-innovation Center for Prevention and Control of Important Animal Infectious Diseases and Zoonoses, [4]Department of Nephrology, Subei People's Hospital, Yangzhou University, [5]School of Chemistry and Chemical Engineering, Yangzhou University, Yangzhou, Jiangsu, People's Republic of China

Correspondence: Lei Fan; Jie Han
School of Chemistry and Chemical Engineering, Yangzhou University, Siwangting Road 180, Yangzhou, 225009, Jiangsu, People's Republic of China
Email fanlei@yzu.edu.cn; hanjie@yzu.edu.cn

Abstract: Nanoparticle drug delivery carriers, which can implement high performances of multi-functions, are of great interest, especially for improving cancer therapy. Herein, we reported a new approach to construct Mn^{2+}-coordinated doxorubicin (DOX)-loaded poly(lactic-*co*-glycolic acid) (PLGA) nanoparticles as a platform for synergistic chemo-photothermal tumor therapy. DOX-loaded PLGA (DOX/PLGA) nanoparticles were first synthesized through a double emulsion-solvent evaporation method, and then modified with polydopamine (PDA) through self-polymerization of dopamine, leading to the formation of PDA@DOX/PLGA nanoparticles. Mn^{2+} ions were then coordinated on the surfaces of PDA@DOX/PLGA to obtain Mn^{2+}-PDA@DOX/PLGA nanoparticles. In our system, Mn^{2+}-PDA@DOX/PLGA nanoparticles could destroy tumors in a mouse model directly, by thermal energy deposition, and could also simulate the chemotherapy by thermal-responsive delivery of DOX to enhance tumor therapy. Furthermore, the coordination of Mn^{2+} could afford the high magnetic resonance (MR) imaging capability with sensitivity to temperature and pH. The results demonstrated that Mn^{2+}-PDA@DOX/PLGA nanoparticles had a great potential as a smart theranostic agent due to their imaging and tumor-growth-inhibition properties.

Keywords: PLGA nanoparticles, polydopamine, chemo-photothermal therapy, smart theranostic agent

Introduction

Chemotherapy continues to be a mainstay in the treatment of a broad spectrum of malignancies, unfortunately it has a wide range of adverse side effects and limitations related to the intrinsic toxicity of the drugs to the normal tissues, such as myelosuppression, immunosuppression, mucositis and alopecia.[1–3] Therefore, combination therapy has been considered as a promising strategy to improve therapeutic efficiency and minimize side effects.[4] For example, chemotherapy has been combined with radiation therapy,[5] gene therapy,[6] magnetic hyperthermia therapy,[7] photothermal or photodynamic tumor therapy.[8,9] Photothermal therapy (PTT) is based on photothermal agents that strongly absorb near-infrared (NIR) light and convert it into cytotoxic heat for tumor treatment, such as indocyanine green,[10] gold nanomaterials[11] or carbon spheres,[12] PTT has been demonstrated as a noninvasive, harmless and highly efficient therapeutic strategy. Due to the limitation of radiant power and penetration depth of NIR light, PTT is often hard to kill tumors completely and might result in a recurrence of tumor growth. To solve this issue, it is expected that high performances of the chemotherapeutic drug and photothermal agent are able to be simultaneously implemented in one single delivery.

submit your manuscript | www.dovepress.com
Dovepress
http://dx.doi.org/10.2147/IJN.S132270

Poly(lactic-*co*-glycolic acid) (PLGA) is one of the most widely used biodegradable polymers as it is able to form stable nanoparticles with a minimal systemic toxicity for drug delivery or biomaterial applications.[13–15] Despite its popularity as a drug carrier, PLGA does not readily interact with cells and thus requires surface modification to attain this ability.[16] However, PLGA functionalization is challenged due to the lack of surface reactivity and technical complexity.[17] Recent research has demonstrated that dopamine polymerization method has been widely exploited in functionalizing various types of substrates, such as polystyrene particles,[18] V_2O_5 nanofibers,[19] SiO_2 and Fe_3O_4 nanoparticles.[20,21] This method can also be used in the modification of PLGA nanodrug carriers, eliminating the complexity and inefficiency involved in traditional functionalization processes.[22] Furthermore, the product of dopamine polymerization method has recently been reported as a photothermal agent because of good biocompatibility and high photothermal conversion efficiency.[23] Rich functional groups (ie, catechol, carboxyl and amino) in polydopamine (PDA) also endow their ability of directly chelating various metal ions. For example, PDA-based materials complexed with Gd^{3+}, Mn^{2+} or Fe^{3+} ions have been reported as magnetic resonance (MR) imaging contrast agents.[24–26] Thus, the method of dopamine polymerization provides a strategy to implement multi-performances in a PLGA-based drug delivery system for cancer treatment.

Compared with Gd-based magnetic contrast agents involved in nephrogenic systemic fibrosis, Mn-based contrast agents have lower intrinsic toxicity.[27] However, Mn-based contrast agents often exhibit lower relaxivity coefficient. Recently, Mn^{3+} incorporated porphysome as a new theranostic agent for the combination of Mn-enhanced MR imaging diagnosis and PTT has been reported,[28] but its relaxivity coefficient (1.2 $mM^{-1}\cdot s^{-1}$) is relatively low. So, how to construct a smart theranostic nanoplatform based on PLGA and Mn^{2+} with both high relaxivity and sensitivity to internal or external triggers in the site of tumor for diagnosis by MR imaging is a great challenge, which has important scientific research value, and wide clinical application prospect.

In this study, a Mn^{2+}-coordinated PLGA-based smart drug delivery system with integration of chemotherapy (doxorubicin [DOX]) and photothermal therapy (PDA) was developed with the MR imaging capability. The developed Mn^{2+}-PDA@DOX/PLGA nanoparticles have several advantages: 1) PLGA core endows the nanoparticles with high drug loading capacity of DOX for tumor chemotherapy; 2) PDA layer can destroy the tumor directly by thermal energy deposition and also can stimulate the chemotherapy by thermal-responsive delivery of DOX to further improve the therapeutic effect; 3) the release of Mn^{2+} ions chelated on nanoparticles as trigged by temperature and pH in tumor microenvironment can show efficient MR imaging performance with high relativity coefficient. These properties make Mn^{2+}-PDA@DOX/PLGA nanoparticles with great potential in tumor combination therapy for further clinical application.

Materials and methods

Materials

PLGA (lactic acid [LA]:glycolic acid [GA] =50:50, molecular weight 15–25 kDa) was purchased from Akina Inc. (West Lafayette, IN, USA). Dopamine hydrochloride and tris(hydroxymethyl)aminomethane were bought from Aladdin (Shanghai, China). Poly(vinyl alcohol) (PVA) was purchased from Acros Organics (Beijing, China). DOX was bought from Sangon (Shanghai, China). Dichloromethane (DCM), dimethyl sulfoxide (DMSO) and ethanol were purchased from Sinopharm Chemical Reagent Co., Ltd (Shanghai, China). MTT (3-[4,5-dimethylthiazol-2-yl]-2,5-diphenyltetrazolium bromide) assay and other biological reagents were purchased from Thermo Fisher Scientific (Waltham, MA, USA). Roswell Park Memorial Institute medium 1640 (RPMI 1640) was purchased from Thermo Fisher Scientific. The 4,6-diamidino-2-phenylindole (DAPI) was obtained from KeyGEN BioTech (Nanjing, China). All other chemicals were of analytical grade. Purified water was produced by a Millipore water purification system.

Preparation of PLGA nanoparticles

One hundred milligrams of PLGA was dissolved in 2 mL DCM using a vortex for 15 min. After PLGA was completely dissolved, 200 μL of H_2O (W_1) was added to PLGA solution (O), and the mixture was sonicated for 3 min to form water in oil emulsion (W_1/O). The above W_1/O emulsion was then added to 10 mL of 5% (w/w) PVA solution and immediately homogenized using a Scientz-IID probe sonicator for 3 min, pulsing for 5 s on and 5 s off at the amplitude of 60%. The mixture was then added to 50 mL of 0.3% (w/w) PVA solution (W_2) to form double emulsion ($W_1/O/W_2$). The obtained $W_1/O/W_2$ emulsion was stirred overnight to evaporate remaining DCM. The PLGA nanoparticles were collected via centrifugation, washed with deionized water three times, and then freeze dried to powder.

Surface modification of PLGA nanoparticles

PLGA nanoparticles were coated with PDA by incubating 10 mg nanoparticles in 10 mL of dopamine hydrochloride

solution in Tris-HCl buffer (10 mmol/L, pH 8.5) for 6 h at room temperature with rotation. Dopamine concentration was fixed at 1.0 mg/mL. PDA@PLGA nanoparticles were obtained by centrifugation and washed three times with deionized water. For surface metal functionalization, $MnSO_4 \cdot H_2O$ aqueous solution (8 mL, 0.1 mol/L) was mixed with 15 mg of PDA@PLGA nanoparticles. After stirring for 24 h at room temperature, Mn^{2+}-PDA@PLGA nanoparticles were collected by centrifugation, washed with deionized water for three times to completely remove the residual metal ions, and then freezing dried to powder.

Synthesis of Mn^{2+}-PDA@DOX/PLGA nanoparticles

For the preparation of Mn^{2+}-PDA@DOX/PLGA nanoparticles, the experimental procedure was the same as the above except that certain amounts of doxorubicin hydrochloride were dissolved in 200 μL H_2O (W_1). Mn^{2+}-PDA@DOX/PLGA nanoparticles were also washed with deionized water three times and freeze dried to powder.

Characterization

Scanning electron microscopy (SEM, S-4800II; Hitachi, Tokyo, Japan) and transmission electron microscopy (TEM) were applied to characterize shape and structure of nanoparticles. Sizes and zeta potentials of PLGA, PDA@PLGA and Mn^{2+}-PDA@PLGA nanoparticles were measured with Malvern Zetasizer (ZS90). Concentration of Mn^{2+} ions was measured by Inductively Coupled Plasma-Atomic Emission Spectroscopy (ICP-AES, Optima 7300DV; PerkinElmer Inc., Waltham, MA, USA). UV-vis absorption spectra were recorded on a U3900 spectrometer (Hitachi). Fourier transform infrared (FTIR) spectra were performed on IRAffinity-1 spectrometer. The X-ray photoelectron spectroscopy (XPS) measurements were measured on an ESCALAB 250Xi X-ray photoelectron spectrometer (ThermoFisher Scientific). The NIR laser was exported using a power density of 1.0 W/cm^2 (MW-GX-808). The temperature of solution was monitored using a digital thermometer with a thermocouple probe (52II).

Drug loading efficiency and in vitro drug release

For DOX loading experiment, 5 mg of Mn^{2+}-PDA@DOX/PLGA nanoparticles was first dissolved in 3 mL of DCM. After that, 10 mL of deionized water was added, and the DOX molecules were preferentially transferred to water phase. Before collecting the aqueous layer, the mixture was vortexed to phase separation. This procedure was repeated three times to maximize extraction of DOX. The concentration of DOX in water phase was compared against a calibration curve obtained using a UV-vis spectrophotometer at 480 nm. For DOX release, 5 mg of Mn^{2+}-PDA@DOX/PLGA was initially dispersed into 3 mL phosphate-buffered saline (PBS) solution, followed by putting them into the dialysis bag (cutoff molecular weight: 7,000 Da). The dialysis bag immersed in 30 mL of PBS buffer dialysis solution (pH 7.4 or 6.0) at different temperatures. Partial release medium (3 mL) was taken out for UV-vis and ICP-AES testing at a given time, followed by addition of free release medium (3 mL) for continuous observation of release behavior.

Photothermal effect in aqueous solution

To study the photothermal effect, 1.5 mL of the Mn^{2+}-PDA@PLGA suspension with different concentrations, in a cuvette, was irradiated using an NIR laser (808 nm, 1.0 W/cm^2) for 10 min. The temperature of the solution was recorded by a digital thermometer.

In vitro MR imaging

Mn^{2+}-PDA@PLGA nanoparticles were dispersed in aqueous solution at different concentrations for in vitro T1-weighted MR imaging and MR relaxometry. The T1-weighted images were acquired with a conventional spin echo acquisition (repetition time =2,000 ms) with an echo time of 200 ms, section thickness of 3 mm in 0.5 T MiniMR systems. The MR relaxometry measurement relaxation time T1 was recorded using an NMI20-Analyst (Suzhou Niumag Corporation).

Cell viability assay

The cell viability was measured by MTT assay. Mouse colon cancer cells (CT26, obtained from experimental cell resource center of Shanghai Institutes for Biological Sciences) and human embryo kidney cells (293T, obtained from experimental cell resource center of Shanghai Institutes for Biological Sciences) were separately cultured in RPMI 1640 medium containing 10% fetal bovine serum and 1% penicillin–streptomycin at 37°C and 5% CO_2. For in vitro cytotoxicity assay, CT26 and 293T cells were seeded into 96-well plates at 1×10^5/well until adherent and then incubated with various concentrations of Mn^{2+}-PDA@PLGA for 24 and 48 h. Ten microliters of 5 mg/mL MTT solution was then added into each well, followed by incubation for 4 h at 37°C in the presence of 5% CO_2. At the end of the incubated time, the nanoparticles and culture medium were removed

and 100 μL of DMSO was added to dissolve the formazan crystals. Finally, the absorbance at 490 nm of each well was recorded by a microplate reader (SYenergy 2) to determine the relative cell viability.

For in vitro chemo-PTT, CT26 cells were seeded into 96-well plates at 1×10^5/well until adherent and then incubated with various concentrations of Mn^{2+}-PDA@PLGA or Mn^{2+}-PDA@DOX/PLGA at 37°C. Then, the cells were exposed to an 808 nm NIR laser at the power density of 1.0 W/cm^2 for 10 min. The relative cell viabilities after photothermal ablation and chemo-photothermal ablation were measured by the same method as described above.

Cellular uptake

To investigate the cellular uptake behavior of Mn^{2+}-PDA@DOX/PLGA nanoparticles, CT26 cells (1×10^5/well) suspended in 1 mL of RPMI 1640 medium were seeded in a 24-well plate with cell climbing slices on the bottom of the plate for 12 h, and then incubated with Mn^{2+}-PDA@DOX/PLGA (the final concentration was 100 μg/mL) at 37°C for 24 h. The cells were then rinsed twice with 0.01% PBS, fixed with 4% paraformaldehyde for 15 min, 0.4% Triton for 5 min and stained with DAPI for 5 min. After rinsing with PBS three times, cell climbing slices were placed on the glass slides and imaged by laser scanning confocal microscopy (LSCM, TLS SP8 STED).

Tumor model

Balb/c mice were obtained from Yangzhou University Comparative Medicine Centre. Animal experiments were performed following protocols approved by Yangzhou University Laboratory Animal Center and the Medical Ethics Committee of Yangzhou University Medical Academy. The Medical Ethics Committee of Yangzhou University Medical Academy approved this research. For the CT26 tumor model, 2×10^6 cells in 100 μL of serum-free RPMI 1640 medium were injected into the back of each female Balb/c mouse by subcutaneous injection. When the tumor size reached ~60 mm^3, in vivo experiments were carried out.

In vivo MR imaging

CT26 tumor-bearing mice were intravenously (IV) injected with Mn^{2+}-PDA@DOX/PLGA at a dose of 20 mg/kg (body weight). After 24 h, T1 weighted animal MR imaging was performed with a special coil and a mouse cradle on a 3.0 T clinical-MRI (GE Healthcare Bio-Sciences Corp., Piscataway, NJ, USA).

Biodistribution of nanoparticles in organs and tumor tissues

CT26 tumor-bearing mice were intravenously injected with Mn^{2+}-PDA@DOX/PLGA (20 mg/kg). After 24 h, they were sacrificed and major organs (heart, liver, spleen, lung and kidney) and tumor tissues were collected and weighed. Organs and tumor tissues were set into the aqua regia solution and heated overnight at 80°C, and then further heated at 130°C for another 2 h. After filtration (acrodisc syringe filters, polytetrafluorothylene membrane, diameter 13 mm, pore size 0.45 μm), the Mn concentrations were measured by ICP-AES.

In vivo PTT

CT26 tumor-bearing mice were divided into four groups when the tumors reached ~60 mm^3 (n=3 for each group): 1) intravenous injection with PBS as the control group; 2) intravenous injection with Mn^{2+}-PDA@PLGA (injection dose: 100 μL, 20 mg/kg, once every 3 days) and irradiated under NIR laser (808 nm, 1.0 W/cm^2, 10 min, 1 time every 3 days); 3) intravenous injection with Mn^{2+}-PDA@DOX/PLGA (injection dose: 100 μL, 20 mg/kg, 1 time every 3 days); 4) intravenous injection with Mn^{2+}-PDA@DOX/PLGA (injection dose: 100 μL, 20 mg/kg, 1 time every 3 days) and irradiated under NIR laser (808 nm, 1.0 W/cm^2, 10 min, 1 time every 3 days). The tumor temperature changes of mice were monitored by a Fluke Ti95_9Hz thermal imaging camera. The tumor sizes were measured every 3 days with a digital calliper and calculated as volume, $V = \text{length} \times \text{width}^2/2$. The relative tumor volume was analyzed according to the formula V/V_0, where V_0 was the tumor volume when the treatment was initiated.

Histology analysis

The female Balb/c mice (4–6 weeks, 20–25 g) were intravenously injected with Mn^{2+}-PDA@PLGA suspension at different doses (12.5, 25 and 50 mg/kg). The mice receiving pure saline were used as the control group. The potential toxicity effects such as a scruffy appearance or abnormal behavior were monitored every day. At the end of feeding (30 days), the mice were sacrificed and then the main organs (heart, liver, spleen, lung and kidney) were taken out and fixed in 4% paraformaldehyde in PBS. The samples were embedded in paraffin, sectioned at a thickness of 3 μm, stained with hematoxylin and eosin (H&E) and then examined using an optical microscope for histopathological analysis.

Statistical analysis

Quantitative data were expressed as the means ± standard deviations.

Results and discussion

The synthesis of Mn^{2+}-PDA@DOX/PLGA nanoparticles is presented in Scheme 1. PLGA nanoparticles were first prepared via a $W_1/O/W_2$ synthetic process.[29] Spherical morphology and smooth surface of PLGA nanoparticles were observed by SEM and TEM images. The SEM image in Figure 1A confirmed that the bare PLGA nanoparticles were uniform. As shown in Table S1, the mean diameter of PLGA nanoparticles was 147.1±3.75 nm with a zeta potential of −15.3±0.28 mV as measured by a particle-size analyzer. Moreover, the smooth surface of the bare PLGA nanoparticle was also confirmed through the TEM image (Figure 1B). Surface modification of PLGA nanoparticles with dopamine was further performed according to our previous work.[30] In this process, the PLGA nanoparticles were first dispersed in Tris-HCl buffer solution (pH 8.5), and then mixed with dopamine. Under weakly alkaline and aerobic conditions, dopamine molecules self-polymerized to form thin adherent PDA on surfaces of PLGA nanoparticles. After coating, the morphology of PDA@PLGA nanoparticles was also examined by SEM and TEM. As shown in Figure 1C, there was no visible surface feature attributable to PDA coating, which might be rationalized by smooth uniform coating of PDA that did not have a significant influence on the spherical shape of PLGA nanoparticles. Through TEM image of PDA@PLGA (Figure 1D), a black layer on the periphery of the PLGA nanoparticle was clearly observed, which was distinguished from the uncoated PLGA nanoparticle, verifying the successful modification of PDA. After modification, the average size of the obtained PDA@PLGA nanoparticles was increased from 147.1±3.75 nm to 198.13±6.23 nm, and the zeta potential was decreased from −15.3±0.28 mV to −12.3±0.28 mV (Table S1). Together, a thin layer (~25 nm) of PDA coating successfully formed on surfaces of the PLGA nanoparticles.

PDA is composed of several basic monomers, such as 5, 6-dihydroxyindole, 5,6-dihydroxyindole-2 carboxylic acid, pyrrole and 3,4-dihydroxyphenylalanine. The *o*-dihydroxyl group of the catechol unit has been proven to form a coordinate complex with metal ions, such as Fe^{3+}, Zn^{2+}, Cu^{2+} and Mn^{2+} ions.[31] Among these metal ions, Mn^{2+} ions have the ability to shorten the longitudinal relaxation T1 times of photons from bulk water as a contrast agent for T1-weighted MR imaging.[32,33] To verify loading Mn^{2+} by intrinsically chelating with PDA, we first tested FTIR and XPS spectra of Mn^{2+}-PDA@PLGA nanoparticles. As shown in Figure S1, before surface modification with PDA, typical PLGA absorption bands at around 1,093 (ν_{C-O}), 1,173 (ν_{C-O}), 1,422 (δ_{C-H}), 1,761 ($\nu_{C=O}$), 2,998 (ν_{C-H}) and 2,953 cm^{-1} (ν_{C-H}) were seen clearly in the FTIR spectrum. After the surface was covered with PDA, new absorbance signals appeared. Peaks at 1,506 and 1,616 cm^{-1} were assigned to amide N–H shearing vibration and benzene skeleton vibration of the PDA, respectively. A typical peak at 3,388 cm^{-1} from vibration of catechol-OH groups showed slight red shift after Mn^{2+} coordination in Mn^{2+}-PDA@PLGA nanoparticles. Moreover, as shown in Figure 1E and F, Mn^{2+}-PDA@PLGA nanoparticles showed a peak at 399.6 eV in XPS spectrum, which corresponded to nitrogen (N1s). This result verified the presence of the PDA layer. Mn peaks at a binding energy of 660.0–663.0 eV demonstrated that Mn^{2+} existed. Close inspection of the XPS spectrum of Mn2p, as shown in Figure 1F, exhibited two peaks at 642.0 and 653.0 eV, which corresponded to the binding energies of Mn2p3/2 and Mn2p1/2, respectively. In addition, as shown in Table S1, compared with PLGA, PDA@PLGA nanoparticles, larger size and lower zeta potential of Mn^{2+}-PDA@PLGA nanoparticles were obtained. This result was attributed to the larger ionic radius and positive charges of Mn^{2+} ions, revealing that Mn^{2+} ions were coordinated onto the PDA@PLGA surfaces. Therefore, the successful incorporation of PDA coating onto the surfaces of PLGA nanoparticles and coordination binding of Mn^{2+} on the surfaces of PDA@PLGA nanoparticles were both obtained.

To explore the possibility of Mn^{2+}-PDA@PLGA nanoparticles as a platform for MR imaging, we diluted Mn^{2+}-PDA@PLGA suspension into four different concentrations for MR scanning using a scanner with a magnetic field of 0.5 T. As shown in Figure 2A, Mn^{2+}-PDA@PLGA suspension showed obvious concentration-dependent brightening effect under T1-weighted MR imaging. The reciprocal values of relaxation times were plotted as a

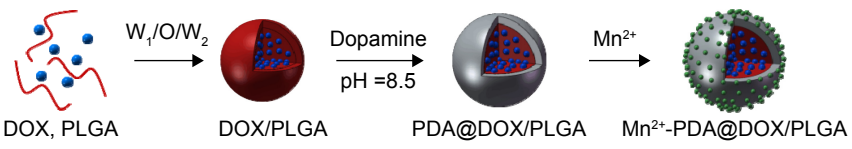

Scheme 1 Schematic diagram of synthesis process of Mn^{2+}-PDA@DOX/PLGA nanoparticles.
Abbreviations: DOX, doxorubicin; PDA, polydopamine; PLGA, poly(lactic-*co*-glycolic acid); $W_1/O/W_2$, $water_1/oil/water_2$.

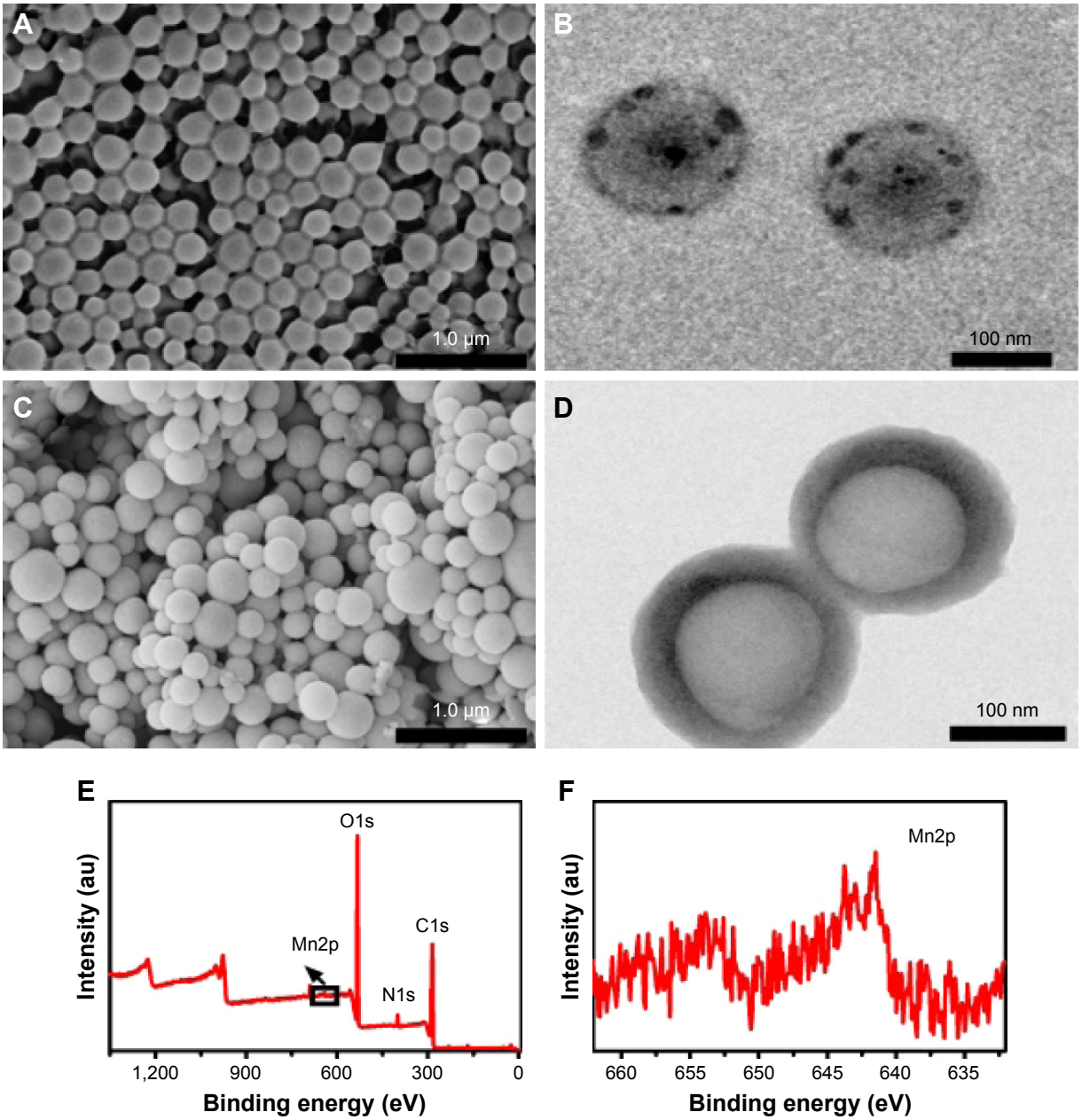

Figure 1 (**A**, **C**) SEM and (**B**, **D**) TEM images of (**A**, **B**) PLGA nanoparticles and (**C**, **D**) PDA@PLGA nanoparticles. XPS patterns of (**E**) Mn^{2+}-PDA@PLGA and (**F**) corresponding deconvoluted Mn2p spectrum of Mn^{2+}-PDA@PLGA; (**F**) is the enlarged view of black box in (**E**).

Abbreviations: PDA, polydopamine; PLGA, poly(lactic-*co*-glycolic acid); SEM, scanning electron microscopy; TEM, transmission electron microscopy; XPS, X-ray photoelectron spectroscopy.

function of Mn^{2+} concentration. As shown in Figure 2B, the relaxation rate (r_1) was determined to be 30.49 $mM^{-1}\cdot s^{-1}$, which was much higher than that of the clinic-approved Gd-based T1 MR contrast agent Magnevist (4.29 $mM^{-1}\cdot s^{-1}$).[34] The significant enhancement in relaxivity for T1-weighted MR imaging may be attributed to characteristic catechol or carboxyl groups on PDA@PLGA nanoparticles, which can enable more water molecules to bond to the Mn^{2+} complex. Next, in vivo MR imaging on mice was carried out. Mice bearing CT26 tumors were IV injected with Mn^{2+}-PDA@PLGA and then imaged under a 3.0 T MR imaging system. An obvious brightening effect could be observed in the tumor region at 24 h postinjection compared with the preinjected image (Figure 2C). Furthermore, the quantitative MR imaging given by region-of-interest quantification also verified the enhancement of T1-weighted MR signals (Figure 2D), confirming that Mn^{2+}-PDA@PLGA is an excellent Mn-based T1-MR contrast agent in vivo. These results also

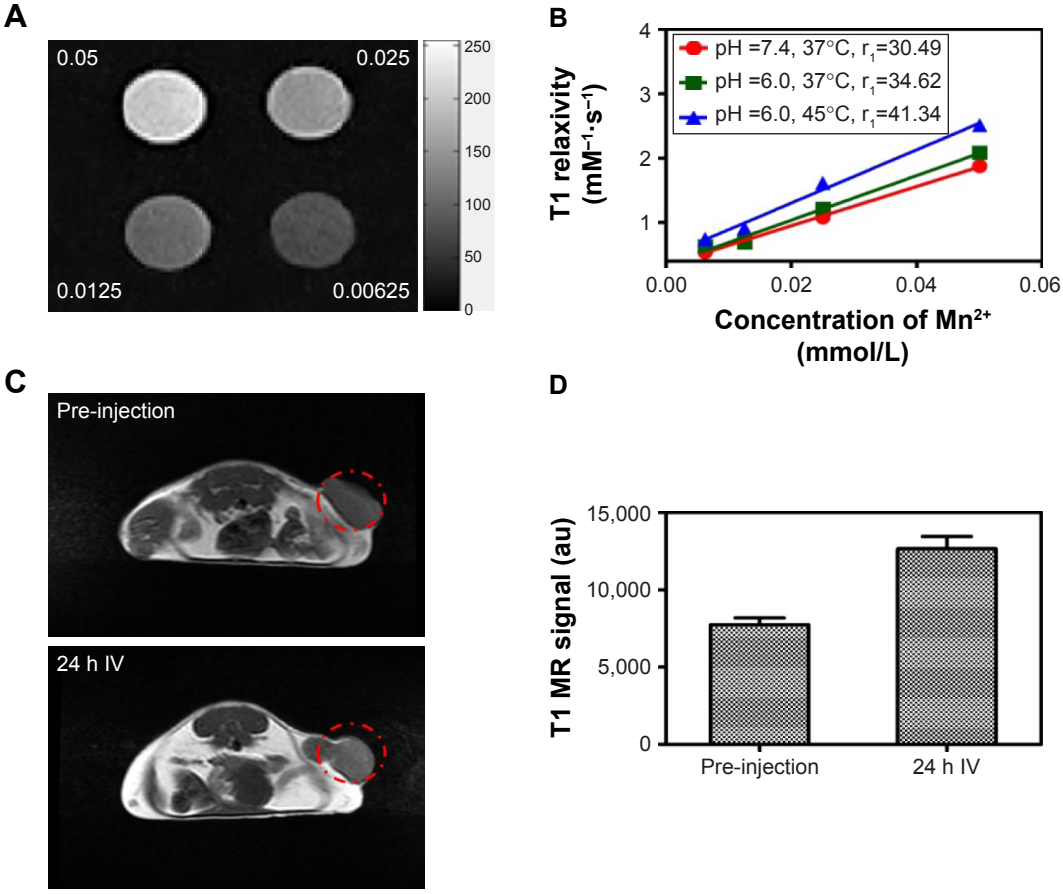

Figure 2 (**A**) T1-weighted MR images of Mn^{2+}-PDA@PLGA at different concentrations of Mn^{2+} (mmol/L). (**B**) The relaxation rates (1/T1) of Mn^{2+}-PDA@PLGA versus different concentrations of Mn^{2+}. (**C**) In vivo T1-weighted MR images of a mouse taken before injection (upper) and 24 h postintravenous injection (bottom) with Mn^{2+}-PDA@PLGA. A brightening effect could be observed in the tumor region. The red circle is the tumor region of the mice. (**D**) T1-weighted MR signals in the tumor before injection and 24 h postintravenous injection with Mn^{2+}-PDA@PLGA.
Abbreviations: PDA, polydopamine; PLGA, poly(lactic-*co*-glycolic acid); MR, magnetic resonance; IV, intravenous.

showed the effective tumor accumulation of the nanoparticles via the enhanced permeability and retention.

To test the photothermal effect of Mn^{2+}-PDA@PLGA nanoparticles, the increase in temperature of Mn^{2+}-PDA@PLGA suspension on NIR laser radiation was measured. PDA is a distinguished PTT agent, which is able to generate heat from light absorption.[35] NIR lasers are preferred over visible lasers in PTT to achieve deeper tissue penetration. The 808 nm wavelength is one of the most frequently used wavelengths in photothermal tumor ablation. As shown in Figure 3A, the photothermal heating photos recorded by an infrared (IR) thermal camera showed that Mn^{2+}-PDA@PLGA nanoparticles had a strong photothermal effect. After irradiation for 10 min, temperature of the Mn^{2+}-PDA@PLGA suspension was increased up to 43°C. In addition, as shown in Figure 3B, the increases in temperature and final solution temperature were proportional to the concentration of Mn^{2+}-PDA@PLGA nanoparticles. A temperature increment of 18.8°C was observed at a particle concentration of 200 μg/mL, while the temperature of pure water was increased by 1°C within 10 min. The results indicated that Mn^{2+}-PDA@PLGA nanoparticles had superior ability of NIR photothermal transduction to serve as a photothermal agent.

In order to overcome the limitation of radiant power and penetration depth of NIR laser, the combination of chemotherapy and phototherapy are tested as a more promising strategy for tumor therapy. PLGA core in the Mn^{2+}-PDA@PLGA nanoparticles endowed the nanoparticles to act as ideal carriers for loading anticancer drugs, protein, siRNA, or other guest molecules.[36] We chose DOX as a model antitumor drug. DOX was loaded into the PLGA core through the $W_1/O/W_2$ synthetic process to obtain Mn^{2+}-PDA@DOX/PLGA nanoparticles. The loading efficiency was estimated to be 9.4% and the loading capacity was 4.7%. The dynamic light scattering measurement (Figure S2) showed the hydrodynamic size of Mn^{2+}-PDA@DOX/PLGA nanoparticles was ~200 nm

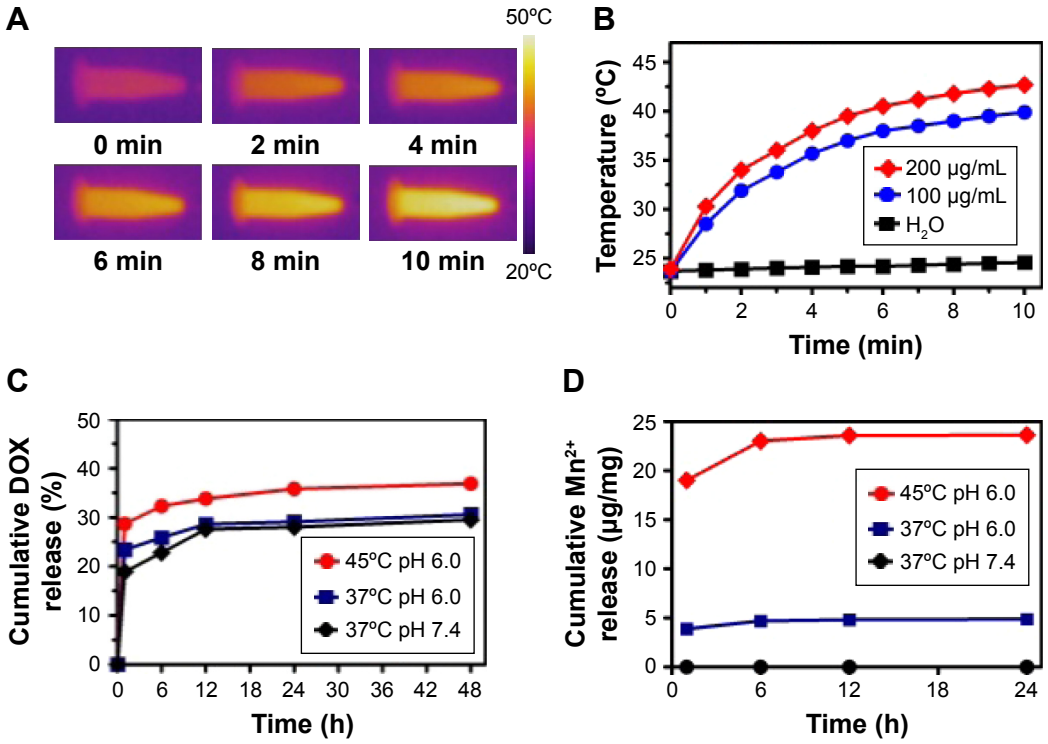

Figure 3 (**A**) Photothermal images of Mn^{2+}-PDA@PLGA suspension (200 μg/mL) after irradiation (808 nm, 1.0 W/cm²) at different times. (**B**) Temperature increase curves for water and Mn^{2+}-PDA@PLGA solutions with an 808 nm laser at a power of 1.0 W/cm². The total irradiation time was 10 min. (**C**) DOX release percentage from Mn^{2+}-PDA@DOX/PLGA at varied pH values and temperatures. (**D**) Mn^{2+} release percentage from Mn^{2+}-PDA@DOX/PLGA at varied pH values and temperatures.
Abbreviations: DOX, doxorubicin; PDA, polydopamine; PLGA, poly(lactic-*co*-glycolic acid).

and these Mn^{2+}-PDA@DOX/PLGA nanoparticles showed excellent stability in serum protein solutions, with almost no precipitate after 24 h (Figure S3). Next, we studied the drug release behavior of Mn^{2+}-PDA@DOX/PLGA nanoparticles in different conditions. As shown in Figure 3C, 48 h later, ~30.6% of DOX released from nanoparticles at pH 6.0 and 37°C, and ~29.5% of DOX released at pH 7.4 and 37°C. This result illuminated that pH change had almost no effect on drug delivery behavior. Such non-sensitive acid-triggered release behavior was owing to the embedment of DOX in the core of PLGA-based nanoparticles, and PLGA molecules were relativity stable in weak acidity condition. We then wondered whether NIR-induced photothermal heating could trigger drug release from nanoparticles. The increase of temperature in the drug-releasing system was utilized to simulate the effect of NIR irradiation. DOX release was enhanced in higher temperature compared to lower temperature. It was observed that only 30.6% DOX was released at 37°C (pH 6.0) after 48 h, while the DOX release percentage was increased by ~6.3% at 45°C (pH 6.0). This result was attributed to the fact that PLGA mesh became loose and the diffusion rate of DOX was enhanced at higher temperature. These two major conditions triggered DOX release with increasing of temperature during chemo-photothermal synergistic therapy. Hence, the Mn^{2+}-PDA@DOX/PLGA nanoparticles showed thermo-sensitivity, and were beneficial to minimize the side effects of chemotherapeutics before reaching lesions, to enhance the antitumor efficiency.

Furthermore, we also used ICP-AES to determine Mn^{2+} concentration in the releasing medium at different pH and temperatures. As shown in Figure 3D, release profiles of Mn^{2+} ions exhibited pH- and thermo-dual triggered behaviors. It was found that Mn^{2+} release amount was increased from 0.67 μg/mg (pH 7.4, 37°C) to 23.62 μg/mg (pH 6.0, 37°C) in 24 h. The results were attributed to the fact that linkage between Mn^{2+} and PDA was broken in lower pH.[37] Compared with Mn^{2+} released at lower temperature, the Mn^{2+} release at higher temperature was also enhanced at the same pH. The stability of coordination bonds in "Mn^{2+}-PDA" architecture at lower pH or higher temperature was weakened, which was the main reason giving rise to the release of Mn^{2+}. Thus, the release of Mn^{2+} ions was triggered by both temperature and pH in tumor microenvironment during the chemo-photothermal synergistic therapy. Compared with Mn^{2+} ions trapped/coordinated into the structure of Mn-based materials, free Mn^{2+} ions showed efficient MR imaging

performance.[38] The r_1 value increased to 34.62 $mM^{-1}\cdot s^{-1}$ when the pH value was reduced to 6.0, and the increasing temperature also favored the r_1 value increase (41.34 $mM^{-1}\cdot s^{-1}$, pH 6.0, 45°C), confirming that Mn^{2+}-PDA@PLGA nanoparticles can be used as an excellent pH- and temperature-responsive Mn-based T1-weighted MR imaging contract agent. Furthermore, PLGA core endowed Mn^{2+}-PDA@PLGA nanoparticles with high antitumor drug loading capacity for tumor chemotherapy. Together, combining the high-efficiency chemotherapy and excellent photothermal conversion property, Mn^{2+}-PDA@DOX/PLGA nanoparticles showed great potential in synergistic chemo-PTT for tumors with an efficient MR imaging performance.

Next, we tested the potential toxicity of Mn^{2+}-PDA@PLGA nanoparticles to two types of cells, including CT26 cells and 293T cells. The relative viabilities of cells after being incubated with Mn^{2+}-PDA@PLGA for 24 and 48 h were determined by MTT assay. As shown in Figures 4A and S4, it was found that Mn^{2+}-PDA@PLGA nanoparticles showed no appreciable negative effect to the cell viability even at high concentration (200 μg/mL). In vitro chemo-phototherapy of Mn^{2+}-PDA@DOX/PLGA was then carried out. For the groups without irradiation, Mn^{2+}-PDA@DOX/PLGA nanoparticles were incubated with CT26 cells for 24 h before the MTT assay. As shown in Figure 4B, Mn^{2+}-PDA@DOX/PLGA nanoparticles induced cytotoxicity to cells, owing to encapsulation of DOX in the core of the nanoparticles. For the groups with irradiation, CT26 cells were incubated with different concentrations of Mn^{2+}-PDA@PLGA or Mn^{2+}-PDA@DOX/PLGA nanoparticles for 12 h, irradiated by an 808 nm laser at power density of 1.0 W/cm^2, and then the cells were incubated for another 12 h before measuring the viabilities by a standard MTT assay. As shown in Figure 4B, with the increasing of concentration of Mn^{2+}-PDA@PLGA or Mn^{2+}-PDA@DOX/PLGA nanoparticles, the cell viabilities were decreased in both groups. However, the treatment effect by Mn^{2+}-PDA@PLGA nanoparticles was not as effective compared with that by Mn^{2+}-PDA@DOX/PLGA nanoparticles. Many more cells were killed using Mn^{2+}-PDA@DOX/PLGA nanoparticles with NIR irradiation. This result confirmed that,

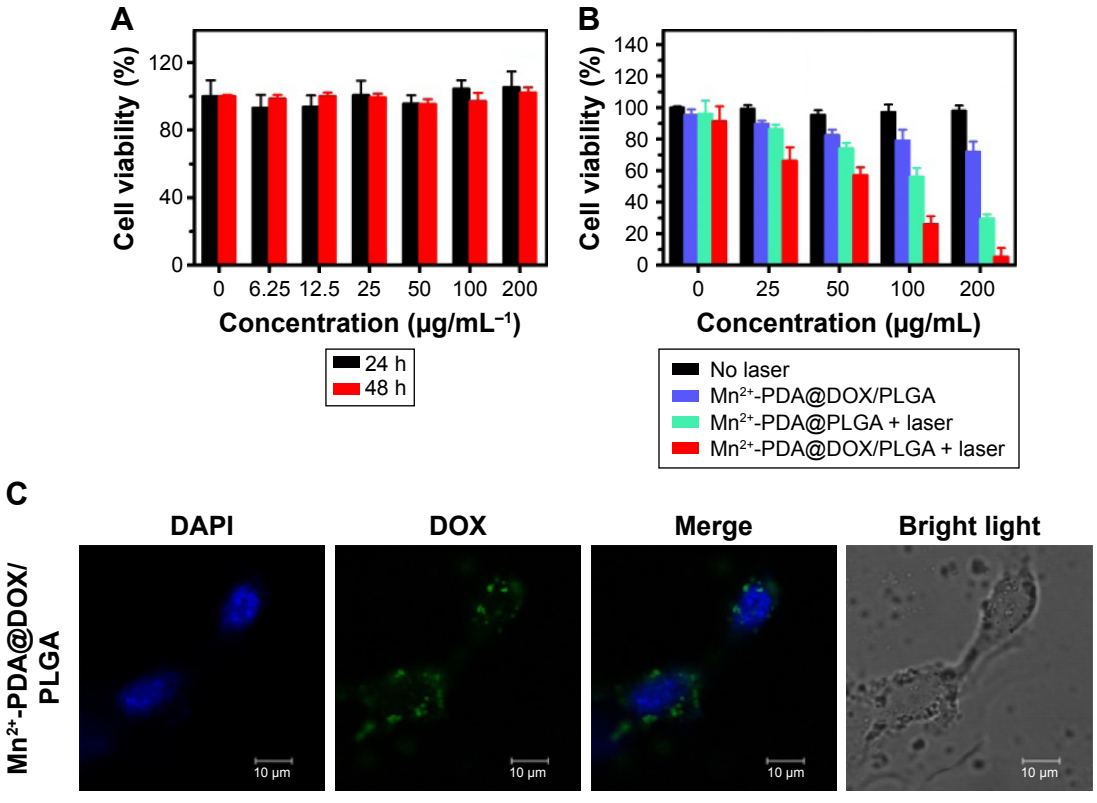

Figure 4 (**A**) Relative viabilities of CT26 cells after being incubated with various concentrations of Mn^{2+}-PDA@PLGA for different times. (**B**) Relative viabilities of CT26 cells incubated with various concentrations of Mn^{2+}-PDA@PLGA and Mn^{2+}-PDA@DOX/PLGA nanoparticles with or without an 808 nm laser irradiation (1.0 W/cm^2) for 10 min. (**C**) Confocal fluorescence images of CT26 cells incubated at 24 h postincubation with Mn^{2+}-PDA@DOX/PLGA.
Abbreviations: DAPI, 4,6-diamidino-2-phenylindole; DOX, doxorubicin; PDA, polydopamine; PLGA, poly(lactic-*co*-glycolic acid).

compared with Mn^{2+}-PDA@PLGA group with irradiation or Mn^{2+}-PDA@DOX/PLGA without irradiation, Mn^{2+}-PDA@DOX/PLGA group with NIR irradiation exhibited much stronger efficacy in killing cancer cells, due to the combination of chemotherapy and PTT. Furthermore, laser scanning confocal microscopy was employed to confirm the cellular uptake of Mn^{2+}-PDA@DOX/PLGA nanoparticles. As shown in Figure 4C, at 24 h postincubation, confocal images showed that the green fluorescence signal from DOX could be detected in the cytoplasm, implying the efficient cellular uptake of the nanoparticles. The above results indicated that the drug-loaded Mn^{2+}-PDA@PLGA nanoparticles had not only an excellent photothermal effect but also a synergistic chemotherapy effect. The high therapeutic efficiency demonstrated wide prospects for this smart nanotheranostic agent for further clinical application.

To investigate the antitumor efficiency of Mn^{2+}-PDA@DOX/PLGA in vivo, comparative efficacy experiments were performed. First, the biodistribution of the Mn^{2+}-PDA@DOX/PLGA nanoparticles following intravenous injection into tumor bearing mice was investigated; the amount of Mn^{2+} localized in the tumor tissues and major organs (spleen, liver, kidney, lung, heart and brain) was determined using ICP-AES at 24 h postinjection (Figure 5A). The data exhibited large amounts of Mn^{2+} accumulated in the reticuloendothelial (liver) and urinary (kidney) systems. Particularly, the content of Mn element in the tumor was over 10.9% injected dose, indicating a higher targeting efficacy of the Mn^{2+}-PDA@DOX/PLGA nanoparticles and thus, the efficacy of PTT can be enhanced. Second, CT26 tumor-bearing mice were divided into four groups, and the treatments for each group are illustrated in "Materials and methods" section. An IR thermal camera was first used to monitor the tumor temperature during the photothermal process. As shown in Figure S5, it was found that surface temperature of the tumor on mice treated with Mn^{2+}-PDA@DOX/PLGA + NIR irradiation rapidly increased from 28°C to 55°C. In contrast, the mice with injection of PBS + NIR irradiation showed no apparent heating effect. This result showed that the Mn^{2+}-PDA@DOX/PLGA nanoparticles kept high photothermal conversion efficiency in vivo. Photographs of the test mice and the tumors in each group after the treatment on the 21st day are shown in Figure 5B and C. Rapid growth occurred in groups 1 and 2. The tumor growth in Mn^{2+}-PDA@DOX/PLGA injected group (group 3) was also partially inhibited. Remarkably, the tumor growth on mice treated with Mn^{2+}-PDA@DOX/PLGA + NIR irradiation (group 4) was greatly inhibited after the combined photothermal therapy and chemotherapy. On the 21st day, mice were sacrificed and tumors were excised. The mean tumor weights in each group after the treatment are shown in Figure 5D. Tumors in group 4 (combination therapy) were much smaller than those in the other three groups, further proving the high efficiency in combination therapy by using Mn^{2+}-PDA@DOX/PLGA with NIR irradiation. To monitor the tumor growth, the length and width of the tumors were measured by digital caliper every 3 days for 21 days. As shown in Figure 5E, the combination therapy group, Mn^{2+}-PDA@DOX/PLGA with laser irradiation, showed significant inhibition of tumor growth. The remaining three treatment groups seemed to have no obvious effect on tumor growth.

The average body weights in each group were recorded and showed no significant variation after treatment, indicating that Mn^{2+}-PDA@DOX/PLGA exerted no acute side effects to the treated mice (Figure 5F). In addition, the major organs of the mice treated with Mn^{2+}-PDA@PLGA were sliced and stained by H&E for histology analysis. As shown in Figure 6, we did not find any appreciable sign of organ damage, inflammatory lesion, or other abnormality, in all major organs of the mice. These preliminary results indicate that Mn^{2+}-PDA@PLGA can possibly be a safe therapeutic agent, considering the low concentration of Mn^{2+} coordinating with PDA@PLGA nanoparticles, as well as the fact that PLGA has been proven to be minimally toxic.

On the basis of our results, we propose a mechanism of enhanced tumor chemo-PTT using our nanoparticles. When Mn^{2+}-PDA@DOX/PLGA nanoparticles reach the tumor region, the nanoparticles strongly absorb NIR light and convert light into heat to remove the tumor through thermal destruction. However, limitation of radiant power and penetration depth of the NIR laser fail to kill the tumor completely. The sustained drug release of DOX acts as a supplement to kill the left over residual cancer cells. Besides using heat to directly destroy the tumor, the photothermal effect of Mn^{2+}-PDA@DOX/PLGA nanoparticles is also utilized to stimulate the chemotherapy by enabling NIR-responsive on demand delivery of drugs for combined cancer treatment. Furthermore, the breaking of the coordination bonds in Mn^{2+}-PDA@DOX/PLGA architecture also responds to the tumor microenvironment to release Mn^{2+} ions with efficient MR imaging performance for tumor diagnosis. These chemo-photothermal synergistic effects of multi-responsive Mn^{2+}-PDA@DOX/PLGA nanoparticles enhance the therapeutic efficacy superior to that obtained by monotherapy.

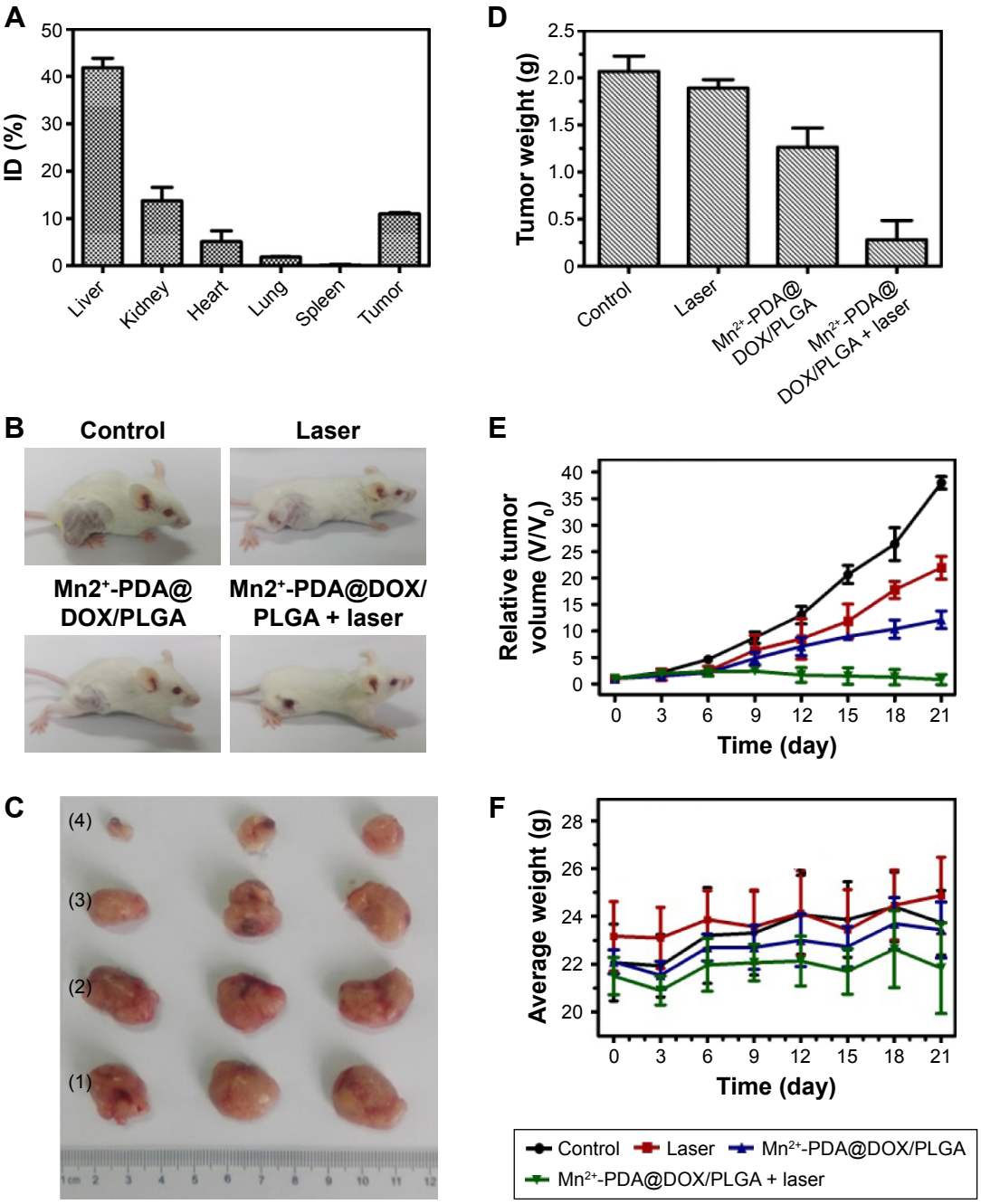

Figure 5 In vivo photothermal therapy of the CT26 tumor bearing mice. (**A**) Biodistribution of Mn^{2+}-PDA@DOX/PLGA in mice. ICP-AES histograms of Mn^{2+} in heart, liver, spleen, lung, kidney and tumor at 24 h postinjection with Mn^{2+}-PDA@DOX/PLGA. (**B**) Representative photos of tumors on mice after various treatments indicated. (**C**) Photos of tumors from (1) control group, (2) laser only group, (3) Mn^{2+}-PDA@DOX/PLGA group, and (4) Mn^{2+}-PDA@DOX/PLGA + NIR group. (**D**) Tumor weights of each group after excision. (**E**) Tumor growth curves of different groups after treatment. The tumor volumes were normalized to their initial sizes. (**F**) The body weight after the various treatments indicated over 21 days.

Abbreviations: DOX, doxorubicin; ID, injected dose; ICP-AES, inductively coupled plasma-atomic emission spectroscopy; NIR, near-infrared; PDA, polydopamine; PLGA, poly(lactic-*co*-glycolic acid).

Conclusion

In summary, we have developed a PLGA-based multifunctional platform as a smart theranostic agent for synergistic chemo-photothermal tumor therapy. Specifically, PDA as a photothermal agent was coated on the surfaces of PLGA nanoparticles, and DOX molecules were loaded in the core of Mn^{2+}-PDA@PLGA nanoparticles. Also, chelation with Mn^{2+} ions further offered our nanoparticles great contrasts in MR imaging. Thus, with these functionalities combined, imaging-guided cancer combination therapy

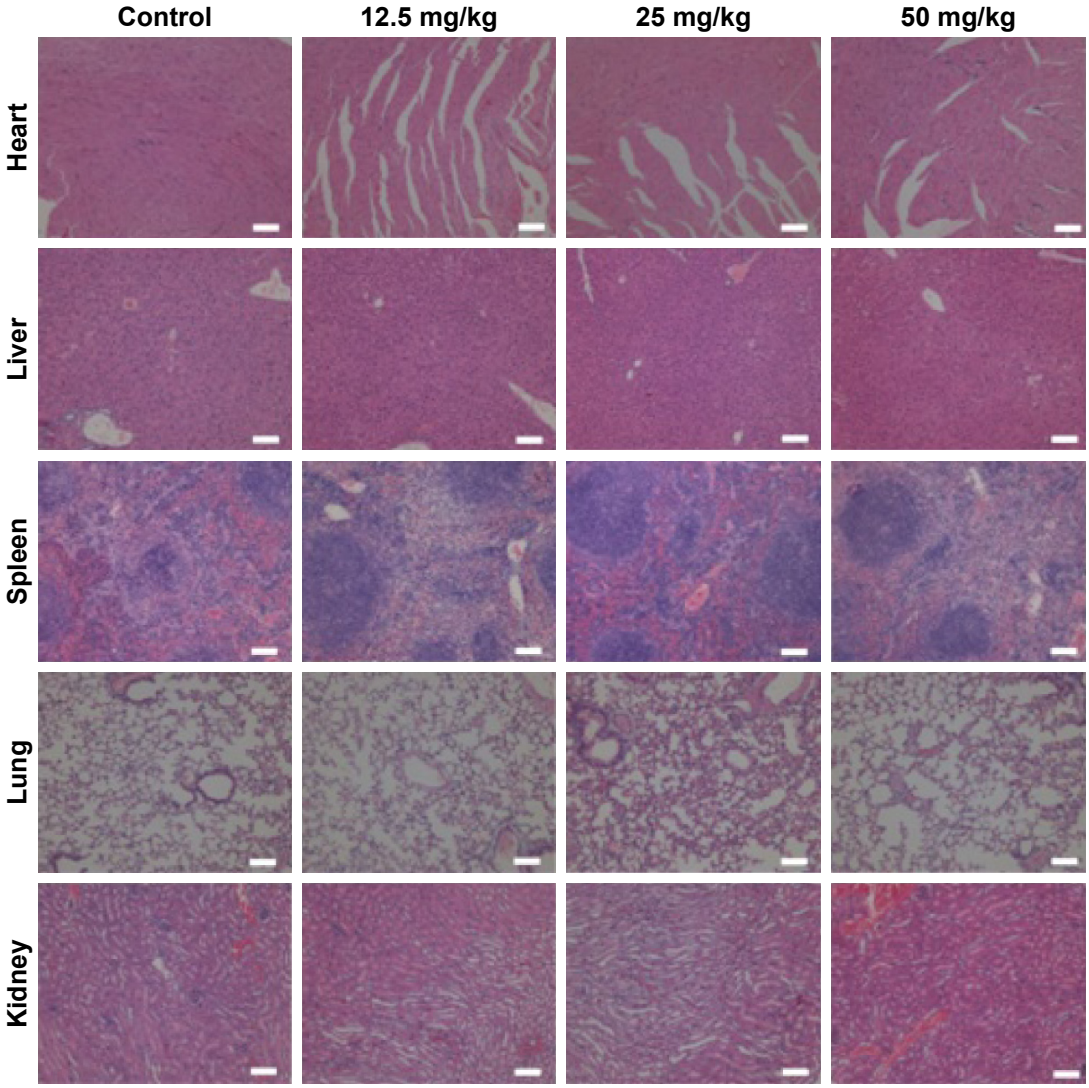

Figure 6 Optical microscopy images of the main organs (heart, liver, spleen, lung and kidney) of Mn^{2+}-PDA@PLGA-treated healthy Balb/c mice after histological hematoxylin and eosin staining. The mice intravenously received Mn^{2+}-PDA@PLGA saline solution at different doses (12.5, 25 and 50 mg/kg) and were fed for 30 days. Scale bars of all images: 100 μm.

Abbreviations: PDA, polydopamine; PLGA, poly(lactic-*co*-glycolic acid).

could be obtained, and a remarkable synergistic effect in destroying tumor was achieved in mouse model experiments. Such a PLGA-based platform showed a number of unique advantages including great biocompatibility, easy and cost-effective fabrication, as well as the capability to load various imaging and therapeutic molecules with high efficiencies.

Acknowledgments

This project was funded by the National Natural Science Foundation of China (Nos 21502165 and 201673202), the Natural Science Foundation of Jiangsu Province (Nos BK20130437 and BK20130439), the University Natural Science Foundation of Jiangsu Province (16KJD150004), the Interdisciplinary Subject Construction Foundation of Yangzhou University (No jcxk 2015-19), the Innovation Foundation of Yangzhou University (No 2015CXJ069) and the Social Development Project of Yangzhou City (YZ2016074), and the Priority Academic Development of Jiangsu Higher Education Institutions.

Disclosure

The authors report no conflicts of interest in this work.

References

1. Coates A, Abraham S, Kaye SB, et al. On the receiving end-patient perception of the side-effects of cancer chemotherapy. *Eur J Cancer Clin Onco*. 1983;19(2):203–208.
2. Lage H. An overview of cancer multidrug resistance: a still unsolved problem. *Cell Mol Life Sci*. 2008;65(20):3145–3167.
3. Semenza GL. Targeting HIF-1 for cancer therapy. *Nat Rev Cancer*. 2003;3(10):721–732.

4. Brannonpeppas L, Blanchette JO. Nanoparticle and targeted systems for cancer therapy. *Adv Drug Delivery Rev*. 2004;56(11):1649–1659.
5. Sher DJ, Rusthoven CC, Khan SA, Fidler MJ, Zhu H, Koshy M. National patterns of care and predictors of neoadjuvant and concurrent chemotherapy use with definitive radiotherapy in the treatment of patients with oropharyngeal squamous cell carcinoma: patterns of care for oropharyngeal cancer. *Cancer*. 2016;123(2):273–282.
6. Mukherjee I, Powell B, Parianos M, Downs D, Ross SB. Available technologies and clinical applications of targeted chemotherapy in pancreatic cancer. *Cancer Genet*. 2016;209(12):582–591.
7. Shen B, Ma Y, Yu S, Ji C. Smart multifunctional magnetic nanoparticle-based drug delivery system for cancer thermo-chemotherapy and intracellular imaging. *ACS Appl Mater Interfaces*. 2016;8(37):24502–24508.
8. Li WT, Peng JR, Tan LW, et al. Mild photothermal therapy/photodynamic therapy/chemotherapy of breast cancer by Lyp-1 modified Docetaxel/IR820 Co-loaded micelles. *Biomaterials*. 2016;106:119–133.
9. He CB, Duan XP, Guo NN, et al. Core-shell nanoscale coordination polymers combine chemotherapy and photodynamic therapy to potential. *Nat Commun*. 2016;7:12499.
10. Chen Q, Xu LG, Liang C, Wang C, Peng R, Liu Z. Photothermal therapy with immune-adjuvant nanoparticles together with checkpoint blockade for effective cancer immunotherapy. *Nat Commun*. 2016;7:13193.
11. Jabeen F, Najam-ul-Haq M, Javeed R, Huck CW, Bonn GK. Au-nanomaterials as a superior choice for near-infrared photothermal therapy. *Molecules*. 2014;19(12):20580–20593.
12. Li L, Chen CF, Liu HY, et al. Multifunctional carbon-silica nanocapsules with gold core for synergistic photothermal and chemo-cancer therapy under the guidance of bimodal imaging. *Adv Funct Mater*. 2016;26(24):4252–4261.
13. Thamake SI, Raut SL, Gryczynski Z, Ranjan AP, Vishwanatha JK. Alendronate coated poly-lactic-co-glycolic acid (PLGA) nanoparticles for active targeting of metastatic breast cancer. *Biomaterials*. 2012;33(29):7164–7173.
14. Park W, Kim D, Kang HC, Bae YH, Na K. Multi-arm histidine copolymer for controlled release of insulin from poly (lactide-co-glycolide) microsphere. *Biomaterials*. 2012;33(34):8848–8857.
15. Xu P, Gullotti, E, Tong L, et al. Intracellular drug delivery by poly (lactic-co-glycolic acid) nanoparticles, revisited. *Mol Pharmaceutics*. 2009;6(1):190–201.
16. Gullotti E, Yeo Y. Beyond the imaging: limitations of cellular uptake study in the evaluation of nanoparticles. *J Control Release*. 2012;164(2):170–176.
17. Amoozgar Z, Park J, Lin Q, Weidle JH, Yeo Y. Development of quinic acid-conjugated nanoparticles as a drug carrier to solid tumors. *Biomacromolecules*. 2013;14(7):2389–2395.
18. Cong Y, Xia T, Zou M, et al. Mussel-inspired polydopamine coating as a versatile platform for synthesizing polystyrene/Ag nanocomposite particles with enhanced antibacterial activities. *J Mater Chem B*. 2014;2(22):3450–3461.
19. Qu KG, Shi P, Ren JS, Qu XG. Nanocomposite incorporating V_2O_5 nanowires and gold nanoparticles for mimicking an enzyme cascade reaction and its application in the detection of biomolecules. *Chem Eur J*. 2014;20(24):7501–7506.
20. Zhang Y, Zhang M, Ding L, Wang Y, Xu J. One-pot method for multifunctional yolk structured nanocomposites with N-doped carbon shell using polydopamine as precursor. *Nanoscale Res Lett*. 2016;11(1):212–218.
21. Si JY, Yang H. Preparation and characterization of bio-compatible Fe_3O_4@Polydopamine spheres with core/shell nanostructure. *Mater Chem Phys*. 2011;128(3):519–524.
22. Park J, Brust TF, Lee HJ, Lee SC, Watts VJ, Yeo Y. Polydopamine-based simple and versatile surface modification of polymeric nano drug carriers. *ACS Nano*. 2014;8(4):3347–3356.
23. Zhang D, Wu M, Zeng Y, Wu L, et al. Chlorin e6 conjugated poly (dopamine) nanospheres as PDT/PTT dual-modal therapeutic agents for enhanced cancer therapy. *ACS Appl Mater Interfaces*. 2015;7(15):8176–8187.
24. Fan Q, Cheng K, Hu X, et al. Transferring biomarker into molecular probe: melanin nanoparticle as a naturally active platform for multimodality imaging. *J Am Chem Soc*. 2014;136(43):15185–15194.
25. Ju KY, Lee JW, Im GH, et al. Bio-inspired, melanin-like nanoparticles as a highly efficient contrast agent for T1-weighted magnetic resonance imaging. *Biomacromolecules*. 2013;14(10):3491–3497.
26. Liu Y, Ai K, Lu L. Polydopamine and its derivative materials: synthesis and promising applications in energy, environmental, and biomedical fields. *Chem Rev*. 2014;114(9):5057–5115.
27. Pan D, Schmieder AH, Wickline SA, Lanza GM. Manganese-based MRI contrast agents: past, present, and future. *Tetrahedron*. 2011;67(44):8431–8444.
28. MacDonald TD, Liu TW, Zheng G. An MRI-sensitive, non-photobleachable porphysome photothermal agent. *Angew Chem Int Ed Engl*. 2014;53(27):6956–6959.
29. Jain AK, Swarnakar NK, Godugu C, Singh RP, Jain S. The effect of the oral administration of polymeric nanoparticles on the efficacy and toxicity of tamoxifen. *Biomaterials*. 2011;32(2):503–515.
30. Xi JQ, Qian XD, Qian KH, et al. Au nanoparticle-coated, PLGA-based hybrid capsules for combined ultrasound imaging and HIFU therapy. *J Mater Chem B*. 2015;3(20):4213–4220.
31. Yeroslavsky G, Richman M, Dawidowicz L, Rahimipour S. Sonochemically produced polydopamine nanocapsules with selective antimicrobial activity. *Chem Commun*. 2013;49(51):5721–5723.
32. Modo M, Hoehn M, Bulte JW. Cellular MR imaging. *Mol Imaging*. 2005;4(3):143–164.
33. Miao ZH, Wang H, Yang H, Li ZL, Zhen L, Xu CY. Intrinsically Mn^{2+}-Chelated polydopamine nanoparticles for simultaneous magnetic resonance imaging and photothermal ablation of cancer cells. *ACS App Mater Interfaces*. 2015;7(31):16946–16952.
34. Rodríguez E, Roig A, Molins E, et al. In vitro characterization of an Fe(8) cluster as potential MRI contrast agent. *NMR Biomed*. 2005;18(5):300–307.
35. Liu Y, Ai K, Liu J, Deng M, He Y, Lu L. Dopamine-melanin colloidal nanospheres: an efficient near-infrared photothermal therapeutic agent for in vivo cancer therapy. *Adv Mater*. 2013;25(9):1353–1359.
36. Markland P, Amidon GL, Yang VC. Modified polypeptides containing γ-benzyl glutamic acid as drug delivery platforms. *Int J Pharm*. 1999;178(2):183–192.
37. Zheng HQ, Gao CB, Peng BW, Shu MH, Che SN. pH-responsive drug delivery system based on coordination bonding in a mesostructured surfactant/silica hybrid. *J Phys Chem C*. 2011;115(15):7230–7237.
38. Cai XJ, Gao W, Ma M, et al. A prussian blue-based core-shell hollow-structured mesoporous nanoparticle as a smart theranostic agent with ultrahigh pH-responsive longitudinal relaxivity. *Adv Mater*. 2015;27(41):6382–6389.

Supplementary materials

Table S1 The sizes and ζ-potentials of PLGA, PDA@PLGA and Mn^{2+}-PDA@PLGA nanoparticles, respectively

Samples	Size (nm)	Zeta potential (mV)
PLGA	147.1±3.75	−15.3±0.28
PDA@PLGA	198.13±6.23	−12.3±0.28
Mn^{2+}-PDA@PLGA	205.7±10.47	−3.83±0.43

Note: Data presented as mean ± standard deviation.
Abbreviations: PDA, polydopamine; PLGA, poly(lactic-*co*-glycolic acid).

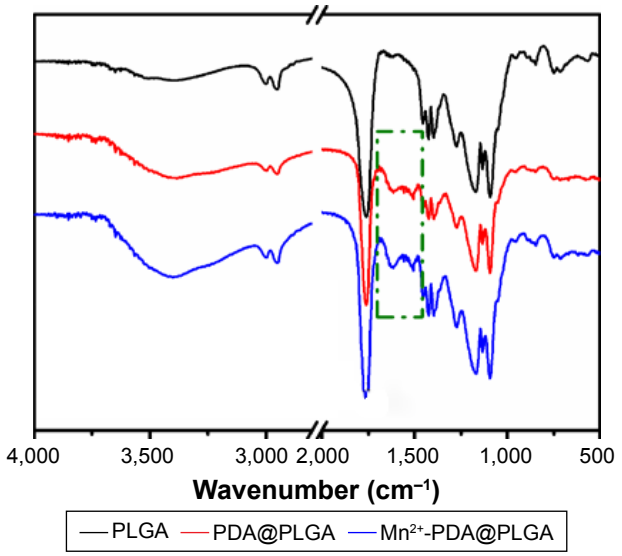

Figure S1 Infrared spectrum curve of PLGA, PDA@PLGA and Mn^{2+}-PDA@PLGA nanoparticles. The difference in spectra of PDA@PLGA and Mn^{2+}-PDA@PLGA nanoparticles mainly appear in the green box.
Abbreviations: PDA, polydopamine; PLGA, poly(lactic-*co*-glycolic acid).

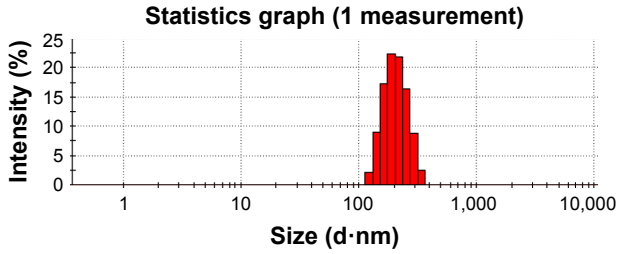

Figure S2 Dynamic light scattering (DLS) data of Mn^{2+}-PDA@DOX/PLGA nanoparticles in aqueous solutions.
Abbreviations: DOX, doxorubicin; PDA, polydopamine; PLGA, poly(lactic-*co*-glycolic acid).

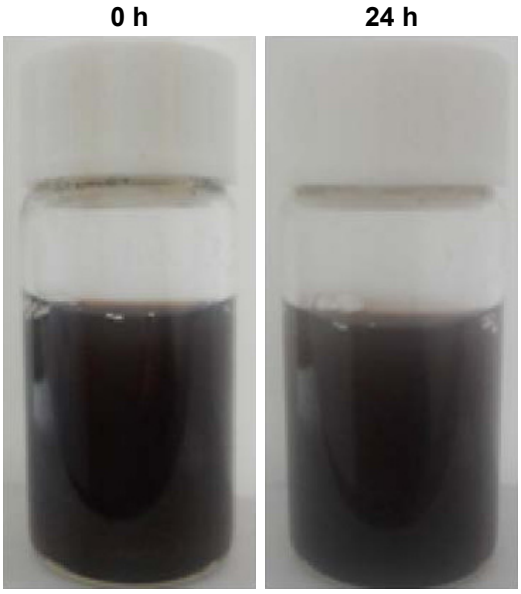

Figure S3 Photos of Mn^{2+}-PDA@DOX/PLGA solutions after 0 h and 24 h.
Abbreviations: DOX, doxorubicin; PDA, polydopamine; PLGA, poly(lactic-*co*-glycolic acid).

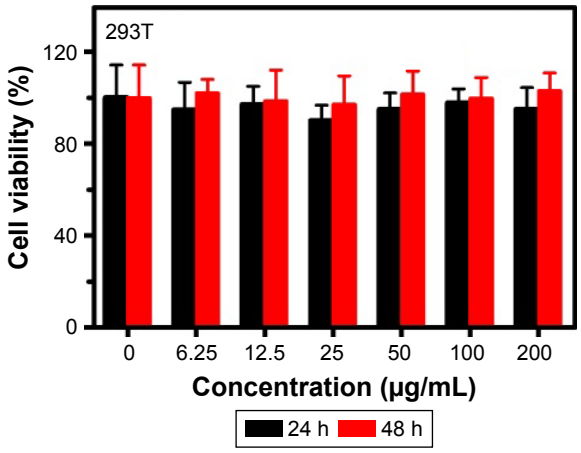

Figure S4 Relative viabilities of 293T cells incubated with Mn^{2+}-PDA@PLGA nanoparticles at various concentrations for 24 and 48 h.
Abbreviations: PDA, polydopamine; PLGA, poly(lactic-*co*-glycolic acid).

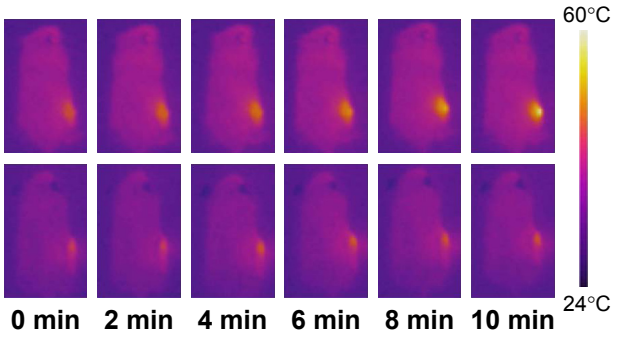

Figure S5 Infrared thermal images of CT26 tumor-bearing mice with NIR laser irradiation (808 nm, 1.0 W/cm², 10 min) after intravenous injection with Mn^{2+}-PDA@DOX/PLGA (top) and PBS (bottom).
Abbreviations: DOX, doxorubicin; PDA, polydopamine; PLGA, poly(lactic-*co*-glycolic acid); NIR, near-infrared.